11th International Conference on Vibration Problems
Z. Dimitrovová *et.al.* (eds.)
Lisbon, Portugal, 9–12 September 2013

BACKWARD WHIRL DURING ROTOR-STATOR CONTACT OF GYROSCOPIC ROTORS

Nicklas Norrick*[1], Benjamin Siegl[1], Oliver Alber[1]

[1]Institute of Structural Dynamics, Technische Universität Darmstadt
Petersenstr. 30, 64287 Darmstadt, Germany
norrick@sdy.tu-darmstadt.de

Keywords: backward whirl, rub, gyroscopics, rotor-stator contact, rotordynamics

Abstract. *For rotor-stator contact of* JEFFCOTT *rotors with flexibly supported rigid stators different motion patterns have been described in previous research. Due to the large amplitudes occuring the most relevant motion pattern to security is backward whirl. Backward whirl can lead to destruction of the whole rotor-stator system. The negative frequency component of the backward whirl was found to be invariant regarding to rotor speed. In contrast to this, the inclusion of gyroscopic effects leads to speed-dependent negative frequency components, previously shown in numerical simulations. Additionally, these results show that more than one backward whirl motion occurs during a single quasi-stationary run-up. In this paper, an analytical approximation for backward whirl for systems with distinctive gyroscopics is developed using an extended* JEFFCOTT *rotor model. Typically, the gap between rotor and stator is very small compared to the backward whirl amplitudes. Because of this, the negative backward whirl frequency component for each chosen rotor speed is very close to a negative natural frequency of the coupled rotor-stator system. Thus, the coupled natural frequency can be used as an approach to solve the equations of motion. This allows the calculation of the resulting backward whirl amplitudes for a rotor with gyroscopic effects at each rotor speed. These results can be used for prediction of contact-induced damages during rotor-stator contact.*

NOMENCLATURE

Latin Symbols		Greek Symbols		Subscripts	
$\boldsymbol{B}$	damping matrix	α	angular eccentricity of the disk	A	contact ring
b	damping coefficient, Ns/m, Nms	δ	instantaneous minimal gap, m	a	axial
$\boldsymbol{f}$	excitation force vector	ε	radial eccentricity, m	b	backward
F	force, N	Θ	moment of inertia, kgm^2	C	contact
$\boldsymbol{G}$	gyroscopic matrix	κ^2	ratio of inertia Θ_p/Θ_a	f	forward
$\boldsymbol{K}$	stiffness matrix	μ	friction coefficient	l	lower
k	stiffness coefficient, N/m, N, Nm	ϕ	complex inclination angle	M	center of mass
M	mass center of the disk	φ	rotation angle of the rotor	N	normal
$\boldsymbol{M}$	mass matrix	Ψ	backward whirl frequency, 1/s	n	n-th
m	mass, kg	ψ	contact point angle	p	polar
$\boldsymbol{N}$	circulatory matrix	Ω	rotor speed, 1/s	R	rotor
$\boldsymbol{q}$	displacement vector	ω	natural frequency, 1/s	RS	rotor + stator ($s=0$)
R	shaft center			S	stator
r	complex displacement, m			U	Unbalance
S	center of the stator			u	upper
s	average nominal gap, m			φ	rotation
y	horizontal axis			Ψ	backward whirl
z	vertical axis			Ω	synchronous

1 INTRODUCTION

When designing rotating machinery, it is generally important to keep the gap between rotor and housing as small as possible, since in fluid machinery, leakage will reduce efficiency; and in electrical machinery, large clearances result in performance losses. However, as the gap between rotating and stationary parts is reduced, the risk of contact increases. Hence, the study of rotor-stator contact has become increasingly important in recent years. The dynamic behavior during rotor-stator contact is particulary important for flexible rotors, as such systems have to tolerate large rotor deflections while crossing the critical speeds. This problem was first mentioned by Taylor [1] and Newkirk [2]. Johnson [3] was the first to describe the synchronous motion of a JEFFCOTT rotor contacting a stator. Black [4] and Ehrich [5] expanded this description to include forward and backward whirl motions containing components with negative frequencies. Subsynchronous motion during contact was first observed by Ehrich [6] and Bently [7]. Sub- and supersynchronous motion patterns of the rotor are examined in detail by Choi and Noah [8]. Up to this point a good overview of the work in this field was given by Muszynska [9]. Later, Ehrich [10] described the occurrence of chaotic behavior. A very comprehensive description of various possible motion patterns and conditions for their occurrence was given by Ehehalt [11]. Special emphasis was placed on forward and backward whirl and on the backward frequency components occurring with these motion patterns. It was found that the negative frequencies of the backward components are almost unaffected by the rotor speed. In general, rotor systems often exhibit gyroscopic effects. The gyroscopic effects cause a splitting of backward and forward natural frequencies. Because of the difference of forward and backward eigenfrequencies additional resonance phenomena occur during rotor-stator contact. These phenomena which have been examined by numerical simulations in previous work [12] are the focus of this paper. To be able to make predictions for the backward whirl frequencies and amplitudes plus the transitions from one motion pattern to another an analytic approach is reasonable.

2 MATHEMATICAL MODEL

Figure 1 shows the extended model used to describe the fundamental behavior of rotor-stator contact for a gyroscopic rotor. The model consists of a JEFFCOTT rotor with distinctive gyroscopics [13], a flexibly mounted rigid stator and a viscoelastic contact model.
The rotor consists of a flexible shaft (stiffness matrix $\boldsymbol{K}$) carrying a rigid disk with the mass matrix $\boldsymbol{M}$ and showing a radial mass eccentricity ε_M (static unbalance) and the angular eccentricity α (couple unbalance). The rotor is externally damped (damping matrix $\boldsymbol{B}$). The gyroscopic effect is described by the gyroscopic matrix $\boldsymbol{G}$ and the circulatory matrix $\boldsymbol{N}$. The displacement vector of the rotor

$$\boldsymbol{q} = \begin{bmatrix} r_R \\ \phi \end{bmatrix} \tag{1}$$

is composed of the complex shaft deflection $r = z + iy$ and the complex shaft inclination $\phi = \varphi_z + i\varphi_y$. The equation of motion of the rotor,

$$\boldsymbol{M}\,\ddot{\boldsymbol{q}} + (\boldsymbol{B}+\boldsymbol{G})\,\dot{\boldsymbol{q}} + (\boldsymbol{K}+\boldsymbol{N})\,\boldsymbol{q} = \boldsymbol{f}_U + \boldsymbol{f}_C, \tag{2}$$

contains on the right hand side the excitation force vector $\boldsymbol{f}_U$ (static and couple unbalance) and the contact force vector $\boldsymbol{f}_C$,

$$\boldsymbol{f}_U = -\begin{bmatrix} \varepsilon_M m_R \\ \alpha(\Theta_a - \Theta_p) \end{bmatrix} \left(e^{i\varphi}\right)^{\cdot\cdot} \qquad \text{and} \qquad \boldsymbol{f}_C = -\begin{bmatrix} F_C \\ 0 \end{bmatrix}. \tag{3}$$

The mass, damping and stiffness matrices are constant,

$$\boldsymbol{M} = \begin{bmatrix} m_R & 0 \\ 0 & \Theta_a \end{bmatrix}, \qquad \boldsymbol{B} = \begin{bmatrix} b_R & 0 \\ 0 & b_{R,\varphi} \end{bmatrix} \qquad \text{and} \qquad \boldsymbol{K} = \begin{bmatrix} k_{11} & -i\,k_{12} \\ i\,k_{12} & k_{22} \end{bmatrix}, \tag{4}$$

whereas the gyroscopic and the circulatory matrices

$$\boldsymbol{G} = \begin{bmatrix} 0 & 0 \\ 0 & -i\Theta_p\dot{\varphi} \end{bmatrix} \qquad \text{and} \qquad \boldsymbol{N} = \begin{bmatrix} 0 & 0 \\ 0 & -i\Theta_p\ddot{\varphi} \end{bmatrix} \tag{5}$$

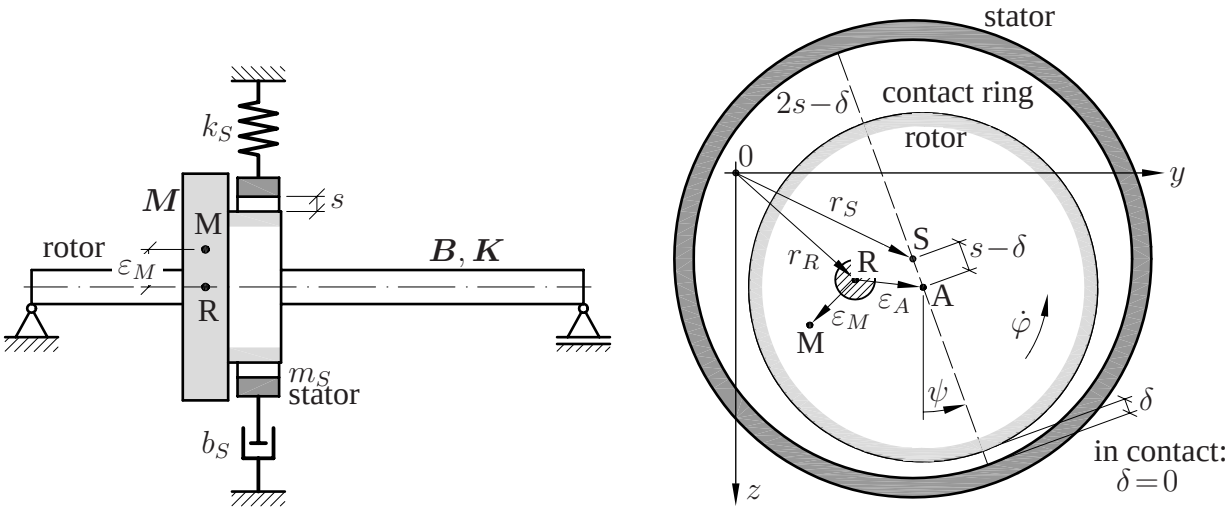

Figure 1: Sketch of the rotor-stator system (left) and kinematic relationships between rotor and stator (right).

depend on the angular velocity $\dot{\varphi}$ and the angular acceleration $\ddot{\varphi}$ of the rotor. The geometric eccentricity of the contact surface on the rotor is ε_A.
The stator (mass m_S) is assumed to be a rigid circular ring supported by isotropic springs (stiffness k_S) and dampers (damping coefficient b_S). The nominal radial clearance between rotor and stator is s. Misalignment between rotor and stator can be considered by the static stator offset $r_{S\,stat}$. If the rotor touches the stator, the distance δ (Figure 1) goes to zero and a contact force F_C is established. Hence, the stator dynamics is described by the equation of motion

$$m_S\,\ddot{r}_S + b_S\,\dot{r}_S + k_S\,(r_S - r_{S\,stat}) = F_C. \tag{6}$$

The nonlinear contact force F_C is composed of a normal component F_{CN} and a tangential component F_{CT}. Assuming a dry friction condition with the COULOMB friction coefficient μ, the contact force is given by

$$F_C = (1 + i\,\mu)\,F_{CN}, \tag{7}$$

as long as the relative circumferential velocity between rotor and stator at the contact point C is positive. Whether rotor and stator contact each other is determined by the distance δ which is described by the kinematic relation

$$r_R - r_S = (s - \delta)\,e^{i\,\psi}. \tag{8}$$

In case of no contact, the angle ψ defines the direction of smallest distance δ; and in case of contact ψ defines the direction of the normal component

$$F_{CN} = |F_{CN}|\,e^{i\,\psi} \tag{9}$$

of the contact force F_C on the stator.
The flexible contact model assumes that the surfaces of rotor and stator can be deformed. Hence, a small penetration of rotor and stator represented by $\delta < 0$ is allowed. The contact force of a flexible contact model depends on the penetration depth $-\delta$ and is described by viscoelastic elements.
Several contact models are discussed in Markert [14], where it is shown that for appropriate contact parameters, the type of the contact model has no significant effect on the calculated global behavior of rotor-stator systems. For the transient numerical studies made by Siegl et. al [12], the normal component of the contact force is assumed to be pseudo-linearly related to the penetration depth $-\delta$ and to the relative normal velocity $\dot{\delta}$ between rotor and stator, i. e.

$$F_{CN} = \Big\langle k_C\,(-\delta) - \langle b_C\,\dot{\delta}\,\rangle \Big\rangle\,\langle -\delta\,\rangle^0\,e^{i\,\psi} \tag{10}$$

where

$$\langle \delta \rangle = \begin{cases} 0 & \text{when} \quad \delta \le 0 \\ \delta & \quad\quad\;\; \delta > 0 \end{cases} \tag{11}$$

is an extended switching function. Equation (11) ensures that on the one hand the contact force is zero for no contact ($\delta > 0$) and that on the other hand no tensile normal forces are applied to rotor and stator. The relevant contact parameters are the contact stiffness k_C and the contact damping b_C. Energy is dissipated only during the restitution phase.
A different way to describe the contact of rotor and stator is the kinematic contact condition

$$r_R - r_S = s\frac{1 - i\mu}{\sqrt{1 + \mu^2}}\frac{F_C}{|F_C|}, \tag{12}$$

which is only valid if rotor and stator are in continuous contact.

3 ANALYTICAL APPROXIMATE SOLUTION

To solve the rotor and stator equations (2, 6) dual-frequency approaches for the complex rotor deflection $r_R(t)$, the complex inclination $\phi_R(t)$, complex stator deflection $r_S(t)$ and the complex contact force $F_C(t)$

$$\begin{aligned} r_R(t) &= \widehat{r}_{R\Omega}\, e^{i\Omega t} + \widehat{r}_{R\Psi}\, e^{i\Psi t} \\ \phi_R(t) &= \widehat{\phi}_{R\Omega}\, e^{i\Omega t} + \widehat{\phi}_{R\Psi}\, e^{i\Psi t} \\ r_S(t) &= \widehat{r}_{S\Omega}\, e^{i\Omega t} + \widehat{r}_{S\Psi}\, e^{i\Psi t} \\ F_C(t) &= \widehat{F}_{C\Omega}\, e^{i\Omega t} + \widehat{F}_{C\Psi}\, e^{i\Psi t} \end{aligned} \tag{13}$$

are made. The synchronous part of the approach is characterized by the term $e^{i\Omega t}$ and the part oscillating with the backward whirl frequency is marked by $e^{i\Psi t}$. If inserted into the equation of motion for the rotor Eq. (2) this approach yields

$$\begin{aligned} &\left[\boldsymbol{K} - \Omega^2 \boldsymbol{M} + i\Omega\,(\boldsymbol{B}+\boldsymbol{G})\right] \widehat{q}_{R\Omega}\, e^{i\Omega t} + \\ &+\left[\boldsymbol{K} - \Psi^2 \boldsymbol{M} + i\Psi\,(\boldsymbol{B}+\boldsymbol{G})\right] \widehat{q}_{R\Psi}\, e^{i\Psi t} = (\widehat{\boldsymbol{f}}_U + \widehat{\boldsymbol{f}}_{C\Omega})\, e^{i\Omega t} + \widehat{\boldsymbol{f}}_{C\Psi} e^{i\Psi t}\,, \end{aligned} \tag{14}$$

and for the stator Eq. (6) it yields

$$\begin{aligned} &[k_S - \Omega^2 m_S + i\Omega\, b_S]\, \widehat{r}_{S\Omega}\, e^{i\Omega t} + \\ &+[k_S - \Psi^2 m_S + i\Psi\, b_S]\, \widehat{r}_{S\Psi}\, e^{i\Psi t} = \widehat{F}_{C\Omega}\, e^{i\Omega t} + \widehat{F}_{C\Psi}\, e^{i\Psi t}\,. \end{aligned} \tag{15}$$

Now the kinematic contact condition Eq. (8) can expanded in the form

$$(\widehat{r}_{R\Omega} - \widehat{r}_{S\Omega})\, e^{i\Omega t} + (\widehat{r}_{R\Psi} - \widehat{r}_{S\Psi})\, e^{i\Psi t} = s\, \frac{1 - i\mu}{\sqrt{1+\mu^2}}\, \frac{\widehat{F}_{C\Omega}\, e^{i\Omega t} + \widehat{F}_{C\Psi}\, e^{i\Psi t}}{|\widehat{F}_{C\Omega}\, e^{i\Omega t} + \widehat{F}_{C\Psi}\, e^{i\Psi t}|}\,. \tag{16}$$

Separation of the synchronous and the asynchronous frequency components in Eqs. (14-16) leads to the equations

$$e^{i\Omega t}\colon \quad \left[\boldsymbol{K} - \Omega^2 \boldsymbol{M} + i\Omega\,(\boldsymbol{B}+\boldsymbol{G})\right] \widehat{q}_{R\Omega} = (\widehat{\boldsymbol{f}}_U + \widehat{\boldsymbol{f}}_{C\Omega}) \tag{17}$$

$$e^{i\Psi t}\colon \quad \left[\boldsymbol{K} - \Psi^2 \boldsymbol{M} + i\Psi\,(\boldsymbol{B}+\boldsymbol{G})\right] \widehat{q}_{R\Psi} = \widehat{\boldsymbol{f}}_{C\Psi} \tag{18}$$

$$e^{i\Omega t}\colon \quad [k_S - \Omega^2 m_S + i\Omega\, b_S] \qquad \widehat{r}_{S\Omega} = \widehat{F}_{C\Omega} \tag{19}$$

$$e^{i\Psi t}\colon \quad [k_S - \Psi^2 m_S + i\Psi\, b_S] \qquad \widehat{r}_{S\Psi} = \widehat{F}_{C\Psi} \tag{20}$$

for the rotor and the stator. Equation 16 yields with the additional postulation $|\widehat{F}_{C\Psi}| \gg |\widehat{F}_{C\Omega}|$

$$e^{i\Omega t}\colon \quad (\widehat{r}_{R\Omega} - \widehat{r}_{S\Omega}) = s\, \frac{1 - i\mu}{\sqrt{1+\mu^2}}\, \frac{\widehat{F}_{C\Omega}}{|\widehat{F}_{C\Psi}|} \quad \text{and} \tag{21}$$

$$e^{i\Psi t}\colon \quad (\widehat{r}_{R\Psi} - \widehat{r}_{S\Psi}) = s\, \frac{1 - i\mu}{\sqrt{1+\mu^2}}\, \frac{\widehat{F}_{C\Psi}}{|\widehat{F}_{C\Psi}|}. \tag{22}$$

Taking Eqs. (18, 20, 22) for frequency Ψ we obtain the complex transfer functions

$$H_{R\Psi} = \frac{\widehat{r}_{R\Psi}}{\widehat{F}_{C\Psi}} = -\frac{(k_{22} - \Psi^2\Theta_a) + i\Psi\,(b_{R\varphi} - i\Omega\Theta_p)}{\det\{\boldsymbol{K} - \Psi^2\boldsymbol{M} + i\Psi(\boldsymbol{B}+\boldsymbol{G})\}} = \\ = -\frac{1}{(k_{11} - \Psi^2 m_R) + i\Psi\, b_R - \dfrac{k_{12}^2}{(k_{22} - \Psi^2\Theta_a) + i\Psi\,(b_{R\varphi} - i\Omega\Theta_p)}} \tag{23}$$

and

$$H_{S\Psi} = \frac{\widehat{r}_{S\Psi}}{\widehat{F}_{C\Psi}} = \frac{1}{(k_S - \Psi^2 m_S) + i\Psi\, b_S}\,, \tag{24}$$

which are defined to eliminate $\widehat{F}_{C\Psi}$, $\widehat{r}_{R\Psi}$ and $\widehat{r}_{S\Psi}$ in the contact force amplitude

$$|\widehat{F}_{C\Psi}| = s\frac{1 - i\mu}{\sqrt{1+\mu^2}}\,\frac{1}{H_{R\Psi} - H_{S\Psi}}\,. \tag{25}$$

Due to a real contact force a condition for the backward frequencies Ψ_{n0} can be obtained by solving the equation (a polynomial of the order of ten)

$$\Im\{|\widehat{F}_{C\Psi}|\} = \sum_{n=0}^{10} a_n \Psi^n \stackrel{!}{=} 0\,. \tag{26}$$

Generally, the roots of polynomials with an order bigger than four can not be calculated analytically [15]. This leads to the use of MATLAB© to obtain the potential backward whirl frequencies. The frequencies have to fulfil certain additional conditions:

1. $\Im\{\Psi_{n0}\} \stackrel{!}{=} 0$, because frequencies have to be real
2. $|\widehat{F}_{C\Psi}(\Psi_{n0})| > 0$ contact force is always positive (no tensile forces)
3. $|\widehat{F}_{C\Psi}(\Psi_{n0})| \gg |\widehat{F}_{C\Omega}|$ to fulfil the assumption to obtain Eqs. (21) and (22) from Eq. (16).

4 RESULTS

These three conditions exclude most of the ten potential backward whirl frequencies resulting from Eq. 26. In the Figures 2 and 3 the remaining frequencies are printed as the solid red lines. They are close to the backward coupled natural frequencies of the rotor-stator system. Additionally, they match the backward whirl frequencies obtained by numerical simulations in the time domain of the rotor in contact (blue). Furthermore, the existence of two different backward whirl frequencies and the fact that there is a transition from one backward whirl motion pattern to another can be predicted (Fig. 3). In both Figures 2 and 3 are dashed and dotted grey lines. The dashed lines show the speed-dependent natural frequencies $\omega_{nf/b}$ of the rotor when not in contact. The dash-dotted lines represent the natural frequencies $\omega_{RS,nf/b}$ of the coupled rotor-stator system. The solid lines are the synchronous Ω and the asymptotic $\Theta_p/\Theta_a\,\Omega$ for the second forward natural frequency ω_{2f} of the rotor with distinctive gyroscopics.

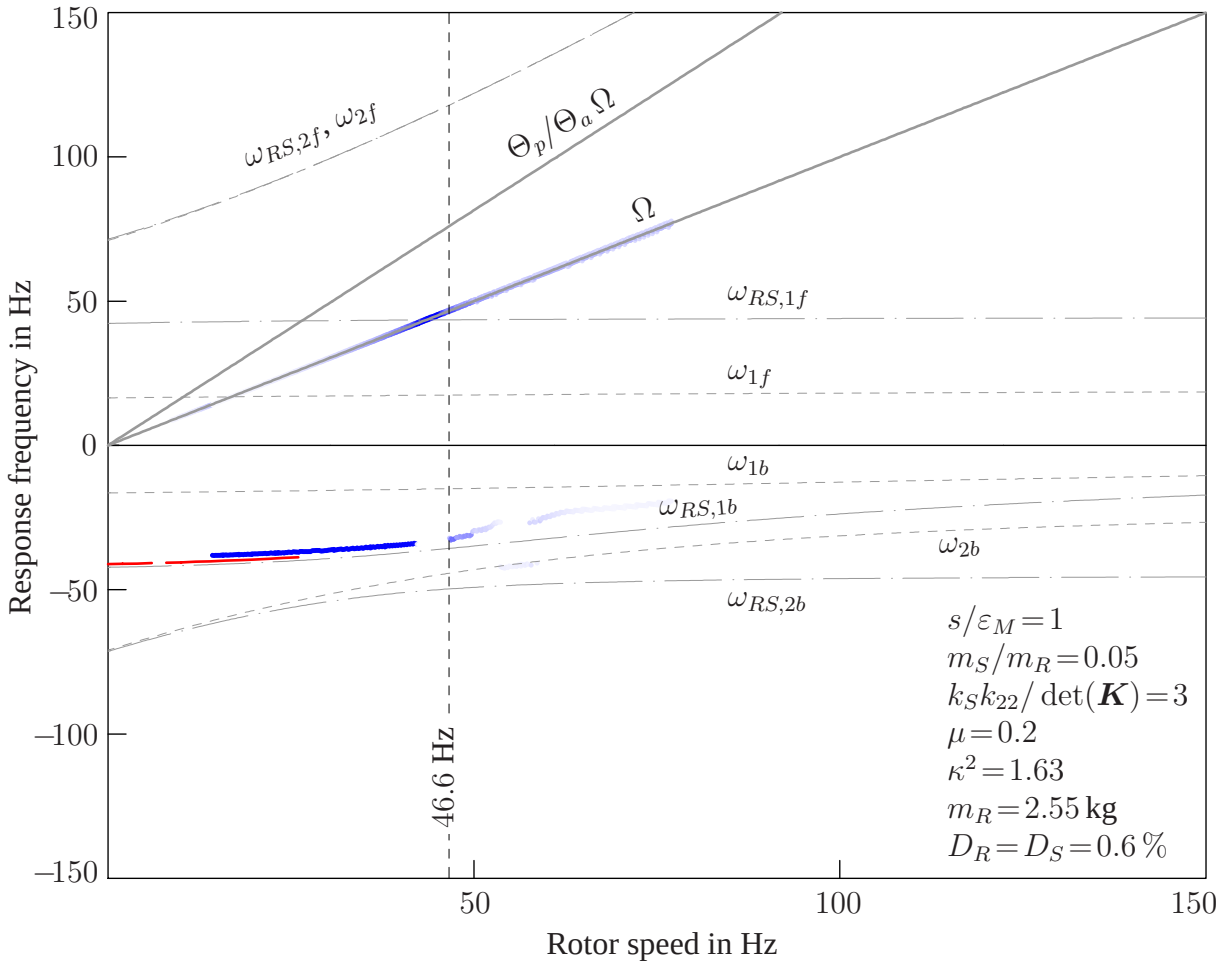

Figure 2: CAMPBELL diagram for the rotor-stator configuration with the narrow gap $s/\varepsilon_M = 1$.

Figure 2 is a CAMPBELL diagram for a slow run-up with a certain rotor-stator configuration which is defined by Ehehalt [16], [11] as a ”light stator”. This means that the first natural frequency of the coupled rotor-stator system in contact reaches resonance in the same frequency band as the stator without contact. For this specific parameter set, synchronous resonance occurs at about $\Omega = 46.6$ Hz due to unbalance excitation. Below the synchronous resonance speed, the rotor-stator system moves in a backward whirl motion as shown in a previous paper [12]. The negative frequency corresponding to the backward whirl obtained by the numerical simulation can be seen in Figure 2 as a blue line. The darker the blue line, the higher the amplitudes of the rotor. Obviously, this frequency component is very close to the first negative natural frequency of the coupled system $\omega_{RS,1b}$ but in the frequency band between the coupled and the uncoupled natural frequency. The red solid line represents the backward whirl frequency component predicted by the analytical method shown in this paper. One can see that it is very close to the results of the numerical simulation. In the numerical study, backward whirl exists for higher rotor speeds than the analytical results predict.

Even more impressive is the result for the ”very light” stator (Fig. 3) created by changing the width of the gap to $s/\varepsilon_M = 20$ and otherwise using the same parameters. This configuration is characterized by a natural frequency of the stator that is lower than the natural frequency of the coupled system. Here, according to the numerical simulation, synchronous resonance occurs at about $\Omega = 42.5$ Hz, again for the system in contact showing a distinctive backward whirl. At a rotor speed of about $\Omega = 70$ Hz the motion pattern jumps to another backward whirl motion

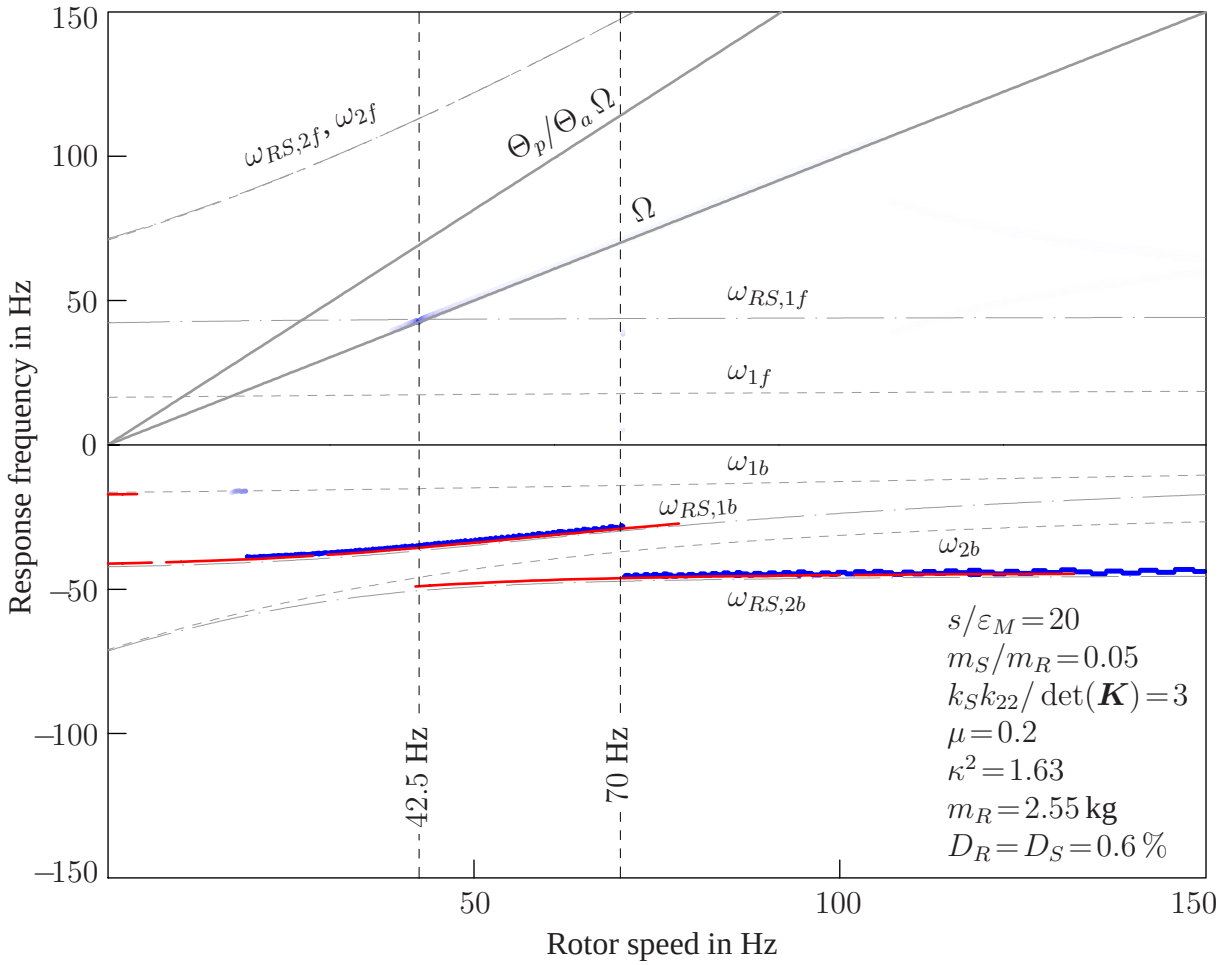

Figure 3: CAMPBELL diagram for the rotor-stator configuration with the wide gap $s/\varepsilon_M = 20$.

pattern with a different negative frequency component. As in the first example, both negative frequency components are close to the respective backward natural frequencies of the coupled system and in the area between those and the respective uncoupled natural frequencies of the rotor. The whirl frequencies predicted by the method shown in this paper are apparent as red solid lines. They are very close to the results of the numerical simulation and coexist in the rotor speed range from 42.5 Hz to above 70 Hz. In this rotor speed range, the transition from one backward whirl motion pattern to another is possible. An criterion for the point of transition is not evident.

The valid solutions Ψ_{n0} are used to calculate the rotor amplitudes $|\widehat{r}_{R\Psi}|$ expected during backward whirl. Fig. 4 shows a comparison of the numerical and analytical results for the second rotor configuration. The gray lines are the result of the numerically simulated run-up of the rotor. The resonance peak is visible at 42.5 Hz as well as the large amplitudes due to backward whirl in the whole rotor speed range from about 20 Hz to 150 Hz. The thick black lines are the amplitude predictions obtained from the analytical approximation. The predicted amplitudes are smaller than the amplitudes obtained numerically. This can be attributed to the neglecting of the synchronous motion due to unbalance excitation throughout the whole rotor speed range. The general shape of the rotor amplitudes during the run-up is predicted nicely.

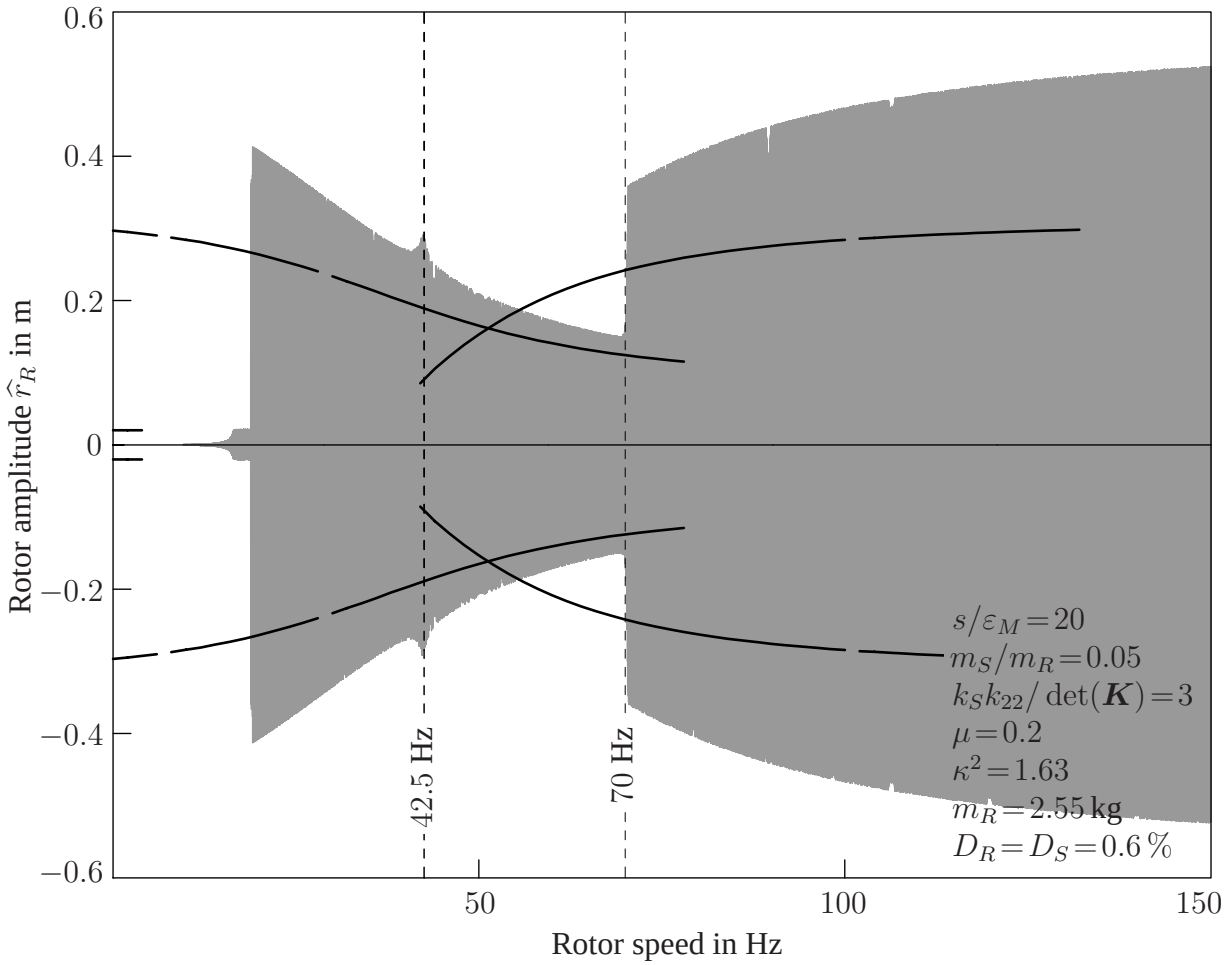

Figure 4: Rotor amplitudes for the rotor-stator configuration with the wide gap $s/\varepsilon_M = 20$.

5 CONCLUSIONS

The method explained in this paper allows the prediction of backward whirl motion patterns, frequencies and amplitudes for rotor-stator contact for rotors with distinctive gyroscopic effects. The results for the negative frequency components match the results of numerical simulations made in a previous paper [12]. Frequency areas for the appearance of transitions between motion patterns can be derived. A comparison between the results of a numerical simulation and the developed semi-analytic approach was drawn. Looking at the rotor amplitudes expected during backward whirl it shows that a reliable amplitude prognosis can only be obtained by the numerical simulation of the rotor-stator system.

The next steps are finding the exact transition frequencies and conditions for the transition from one motion pattern to another for the gyroscopic rotor-stator system.

REFERENCES

[1] H. D. Taylor, *Rubbing shafts above and below the resonance speed (critical speed)*. General Electric Company, R-16709, Schenectady, NY, 1924.

[2] B. L. Newkirk, *Shaft rubbing: relative freedom of rotor shafts from sensitiveness to rubbing contact when running above their critical speeds*. Mechanical Engineering, Vol. 48, pp. 830-832, 1926.

[3] D. C. Johnson, *Synchronous whirl of a vertical shaft having clearance in one bearing*. Journal of Mechanical Engineering Science, Vol. 4, No. 1, pp. 85-93, 1962.

[4] H. F. Black, *Interaction of a whirling rotor with a vibrating stator across a clearance annulus*. Journal of Mechanical Engineering Science, Vol. 10, pp. 1-12, 1968.

[5] F. F. Ehrich, *The dynamic stability of rotor/stator radial rubs in rotating machinery*. ASME Journal of Engineering for Industry, Vol. 91, pp. 1025-1028 , 1969.

[6] F. F. Ehrich, *Subharmonic vibration of rotors in bearing clearance*. ASME Paper 66-MD-1, pp. 1-4, 1966.

[7] D. E. Bently, *Forced subrotative speed dynamic action of rotating machinery*. ASME Paper 74-PET-16, pp. 1-8, 1974.

[8] Y. Choi and S. T. Noah, *Nonlinear Steady-State Response of a Rotor-Support System*. Journal of Vibration, Acoustics, Stress, and Reliability in Design, Vol. 109, pp. 255-261, 1987.

[9] A. Muszynska, *Rotor-to-Stationary Element Rub-Related Vibration Phenomena in Rotating Machinery – Literature Survey*. Shock and Vibration Digest, Vol. 21, No. 3, pp. 3-11, 1989.

[10] F. F. Ehrich, *Observation of subcritical superharmonic and chaotic response in rotordynamics*. Journal of Vibration and Acoustics, Vol. 114, pp. 93-110, 1992.

[11] U. Ehehalt, *Bewegungsformen elastischer Rotoren bei Statorkontakt*. Dissertation TU Darmstadt, 2008.

[12] B. Siegl, N. Norrick and R. Markert, *Theoretical Investigations on Rotor-Stator-Contact of Rotors with Distinctive Gyroscopic Effects*. DINAME 2013 – Proc. of the XV International Symposium on Dynamic Problems of Mechanics, Búzios, Brazil , 2013.

[13] R. Nordmann and H. Pfützner, *Rotordynamik*. Springer Berlin Heidelberg, 2nd Edition, 2001.

[14] R. Markert and G. Wegener, *Transient Vibrations of Elastic Rotors in Retainer Bearings*. Proc. of ISROMAC-7, Vol. 2, pp. 764-774, 1998.

[15] I. N. Bronstein, K. A. Semendjajew, G. Musiol, H. Mühlig, *Taschenbuch der Mathematik*. 6. Auflage, Verlag Harri Deutsch, Frankfurt (Main) , 2005.

[16] U. Ehehalt, E. Hahn and R. Markert, *Motion patterns at rotor stator contact*. Proc. of ASME International Design Engineering Technical Conferences and Computers and Information in Engineering Conference (IDETC/CIE), pp. 1031-1042, 2005.